# Application of Electro-Spark Deposition as a Joining Technology

*The implicit high cooling rates and low individual splat volumes associated with electro-spark deposition facilitate joints in both difficult-to-weld materials as well as dissimilar material combinations*

**BY J. GOULD**


## ABSTRACT

Electro-spark deposition (ESD) has long been used as both a repair and coating technology for a range of material systems. Applications have ranged from repair of Ni-based superalloys to deposition of carbide coatings onto steel cutting blades. The technology is unique in that deposition is accomplished by individual splats of material from the electrode onto the substrate. The scale of these splats is sufficiently small to result in extremely high cooling rates. These high cooling rates have facilitated deposition of difficult to work with materials. In addition, the process has allowed application onto widely disparate dissimilar materials systems. In this work, the technology has been evaluated for direct welding in two candidate applications. These include a nano-stabilized stainless steel for fusion energy applications, and refractory metal to cast Ni-based superalloy combinations for nuclear space propulsion. Sample joints were fabricated for each of these applications, and assessed using metallographic and mechanical testing techniques. Joints on the nano-stabilized steels retained the fine character of the substrate, albeit with some coarsening of the stabilizing precipitates. Joints between the refractory metals and cast Ni-based superalloy were done with a Hastelloy® X filler. Joints showed minimum reaction zones, and properties characteristic of the softer of the two materials joined. Results are discussed in light of the rapid thermal cycles associated with the process, as well as those from other impulse techniques [percussion welding, magnetic pulse welding (MPW)]. Joint morphologies are described in terms of rapid solidification and solid-state phase transformation suppression. Metallurgical and productivity implications are then discussed, and criteria for potential applications described.


## Introduction

Electro-spark deposition (ESD) is a microwelding process that uses rapid electrical power discharges to accomplish metal transfer from an electrode to a contacting substrate. Typically, the process is conducted with a capacitive discharge power supply that provides the short-duration current pulses (10–400 μs). These current pulses are supplied at a range of frequencies ranging from a few hundred to a few thousand hertz. The electrode itself is generally integrated into some device creating high-speed motion relative to the substrate. Examples include both rotating and vibratory approaches. The applied current pulse combined with the intermittent contact (associated with the high relative contact velocity) results in extremely rapid heating, with subsequent localized transfer of material from the electrode to the substrate.

Electro-spark deposition was first defined as early as 1924 (Ref. 1), where it was used for local deposition of martensitic coatings on steels. From the 1940s to the present day, this process has been investigated primarily for a range of coating applications (Refs. 2–7). Initial work with ESD used capacitive-discharge power sources, where motion of the electrode created the resulting charge and discharge cycles. In more recent years, Si-controlled rectifier (SCR) and insulated gate bipolar transistor (IGBT) circuitry have been used (in conjunction with either resistor-capacitor (RC) type analog or microprocessor-based triggering) to create more rapid and reproducible charging and discharging of the capacitors, with subsequent improvements in deposition rates (Ref. 6). As suggested above, various motion mechanisms have also been explored, including vibratory, translational, and rotational modes (Refs. 2–4). The resulting combination of processing and electrode motion conditions has resulted in uneven coating thicknesses of up to 1 mm (Ref. 4).

Through this work, ESD has also been shown to be sensitive to a wide range of material, process, environmental, and torch motion conditions (Ref. 2). It is also of note that there are trade-offs between deposition rates and quality. It has been reported (Ref. 4) that above a deposition thickness of roughly 100 μm, a phenomenon termed "lumping" occurs. Lumping is defined by a nonuniform coating, with localized heavy deposition of material. Lumping appears to be a progressive process (areas of lumping appear to continue to receive preferential deposition of material) and is strongly affected by the quality of the shielding gas. For most applications, both high deposition rates and good surface finish are necessary if the process is to be used effectively.

Electro-spark deposition is commonly used for repair and buildup of Ni-based superalloys (Refs. 8, 9). Current ESD practices for such applications allow dep-


**KEYWORDS**

Electro-Spark Deposition
Nano-Stabilized Materials
Dissimilar Material Joining
Refractory Metals


*J. GOULD* (jerry_gould@ewi.org) *is technology leader, Resistance and Solid State Welding, Edison Welding Institute, Columbus, Ohio.*

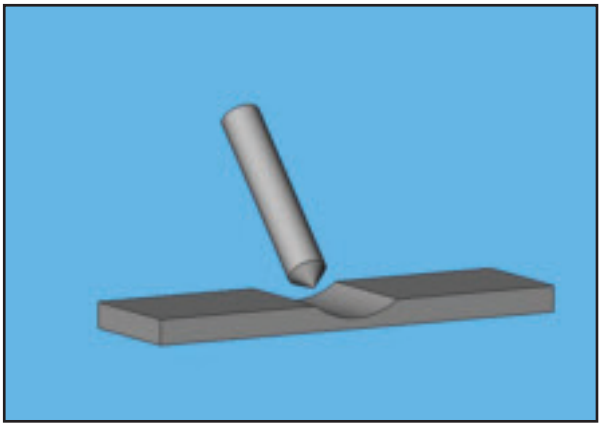

*Fig. 1 — Schematic representation of the configuration used for ESD welding.*

*Fig. 2 — ASAP power supply and torch used for this study.*


*Fig. 3 — Augmented shielding used in the ESD welding MA957 trials.*

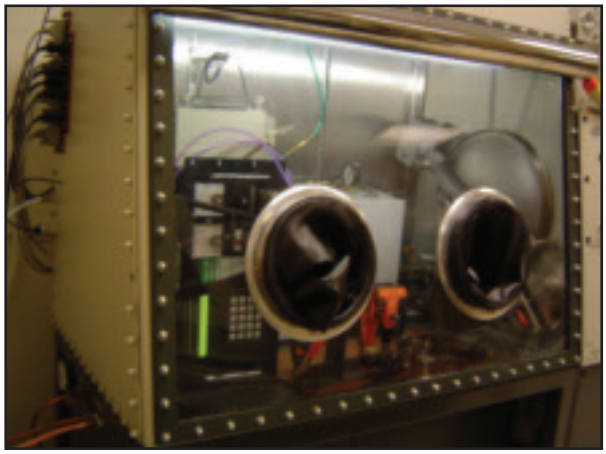

*Fig. 4 — Glove box used for the refractory metal to Ni-based superalloy ESD welding trials.*

osition rates up to 10 mg/min (Refs. 8, 9). The low deposition rates implicitly associated with this technology generally relegate the approach to surface repairs. However, analysis of these repairs indicates both high as-deposited properties minimal metallurgical defects (Ref. 9).

A key advantage of ESD is the rapid thermal cycles associated with the technology. Metallurgical assessments of deposits made with ESD have demonstrated that a single pass typically results in a layer thickness of from 1 to 5 μm (Ref. 9). Previous work has suggested cooling rates in the range of $10^{5}$°C/s to $10^{6}$°C/s (Ref. 9). Cooling rates of this magnitude are considerably outside the range of other conventional joining processes (Ref. 10). Rather, these cooling rates more are consistent with impulse methods such as percussion welding (Ref. 11), and magnetic pulse welding (MPW) (Ref. 12). Microstructural observations in Ni-superalloy deposits also demonstrate similarities with those from percussion welding (Ref. 11) and MPW (Refs. 13, 14).

Electro-spark deposition, percussion welding, and MPW all can be considered variants of "impulse" technologies. Each is essentially driven by capacitively stored electrical energy, occurs over an effective discharge cycle in the range of 10s to 100s of microseconds, and results in resolidified molten zones with thicknesses in the range of microns. It is of interest that percussion and MPW are commonly applied to both difficult to join and dissimilar material combinations (Ref. 15).

In this work, the use of ESD on two specific material combinations is addressed. The first is joining of mechanically alloyed steels. Nano-structured ferritic alloys (NFAs) are currently under consideration for fusion energy applications (Ref. 16). These materials of nominally a ferritic stainless steel composition, stabilized by a high density of Y-Ti-O precipitates. A typical alloy is MA957. Materials are mill ground into powders (Fe-14Cr-W-Ti and $Y_2O_3$), and hipped or extruded for final consolidation. This results in a high density of nano features, largely based on the Y-Ti-O composition, with particle sizes ranging up to ~8 nm. These materials show excellent tensile and creep strengths, as well as offer potential for mitigating radiation effects (Ref. 17). Joining is a challenge with these materials. Thermal processing associated with most welding processes is anticipated to coarsen the precipitates and negate their effectiveness as strengthening mechanisms. Electro-spark deposition was considered here, largely to assess the influence of the rapid heating and cooling rates on coarsening characteristics of the Y-Ti-O precipitates.

The second application addresses joining high-volume fraction gamma prime Ni-based superalloys to refractory metals. The primary application here is for space nuclear propulsion (Ref. 17), allowing a transition from the refractory metal-based reactor to a high-temperature Ni-based superalloy turbine. Concepts for space nuclear propulsion in the early 21st century have incorporated high-temperature Brayton cycles with working fluid temperatures on the order of 850°C (Ref. 17). Concept designs involve a refractory metal-based nuclear reactor as the heat generation source, and a Ni-based superalloy Brayton cycle turbine for mechanical power generation. Candidate materials

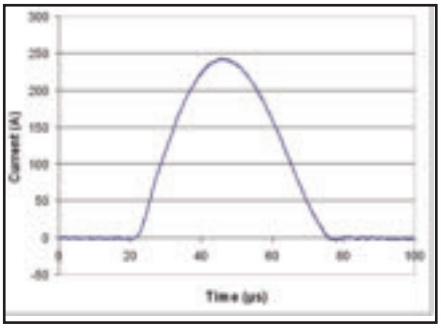


*Fig. 5 — Current waveform for an individual pulse when ESD welding T-111 to MarM 247 with a Hastelloy®–X filler.*

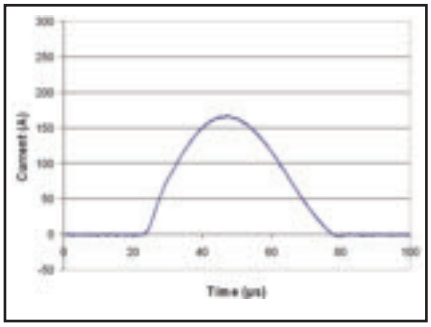


*Fig. 6 — Current waveform for an individual pulse when ESD welding Mo-47%Re to MarM 247 with a Hastelloy®–X filler.*

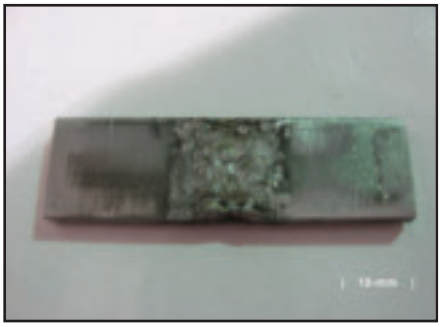

*Fig. 7 — ESD-welded MA957 specimen.*

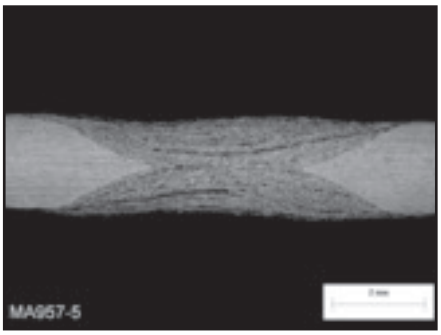


*Fig. 8 — Macrostructure of the ESD-welded MA957 joint.*

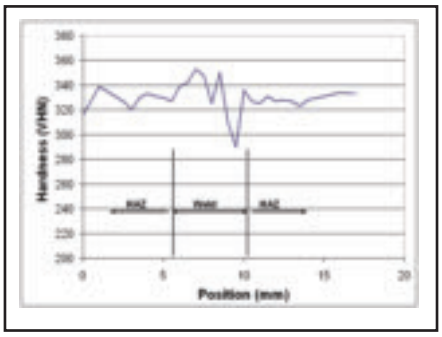


*Fig. 9 — Hardness variations across an ESD joint on MA957.*

for the reactor itself include Mo-Re and Ta-W alloys. Materials for the turbine range from wrought to cast Ni-based superalloys. Metallurgically, bonding of either Mo- or Ta-based systems to Ni-based systems is problematic. In both cases, there are disparities in melting points, low-melting eutectics, and a range of intermetallic compounds. The presence of eutectics is problematic since this can lead to solidification cracking in the fusion zone, as well as liquation cracking in the heat-affected zone (HAZ). Brittle, intermetallic formation can lead to poor mechanical performance in the weld area. These concerns largely rule out conventional fusion welding processes for these applications. Electro-spark deposition was considered for joining these materials largely based on the success of other impulse welding approaches (MPW, percussion welding) for joining such disparate material combinations.

## Experimental Procedures

Electro-spark deposition welding was demonstrated for the MA957 application on material specimens nominally 10 mm wide, 17 mm long, and 2 mm thick. Samples were placed together in a butt configuration, and a scalloped joint prep, nominally 1.2 mm deep with a 6-mm radius, was used. The welding electrode was nominally 3 mm in diameter, 100 mm long, and made of matching material. The assembly configuration is shown in Fig. 1. The electrode itself was prepared with a nominal 90-deg included angle at the tip for these trials. The ESD unit is shown in Fig. 2. This is an ASAP unit with hand-held torch. Deposition conditions are provided in Table 1. Processing paralleled previous work on Ni-based alloys (Ref. 9). Deposition was done with augmented cross-flow shielding as shown in Fig. 3. The weld was completed by first creating layers of material to fill the scalloped joint prep. The joint prep was then repeated on the reverse side, and then filled using the developed ESD practice. Total time for assembly of this joint was on the order of several hours. Resulting specimens were examined through metallographic inspection, hardness testing, and limited tensile testing. Metallographic sectioning and preparation was done using standard techniques. Samples were examined in the unetched condition. These samples were also used for Vickers hardness testing. This was done on a LECO system with a 1-kg weight. Tensile testing was done on a single specimen, transversely across the weld. The specimen used a reduced gauge section, nominally 5.3 mm wide by 1.7 mm thick. This preparation resulted in machined surfaces at the faces and edges of the gauge area. Tensile testing was done at 1.27 mm/min, recording loads to failure.

**Table 1 — Parameters Used for ESD Welding MA957 Sheet**

| | |
|---|---|
| Pulse Rate | 400 Hz |
| Capacitance | 50 µF |
| Voltage | 150 V |
| Electrode Rotation | 1200 rev/min |
| Primary Amperage | 6 A |

The refractory metal to Ni-based superalloy trials were done with two configurations. These included two refractory metal alloys, T-111 (Ta-8%W-2%Hf) and Mo-47%Re, each welded to a cast Ni-based superalloy (MarM-247). Samples for joining were prepared as ½ tensile specimens. Materials were nominally 0.5 mm thick, with a 13-mm base width, reduced to 6 mm in the gauge area. Actual joint prep was again a scallop configuration, similar to that described above. In this case, the scallop was 0.35 mm deep with a 3-mm radius. The welding electrode in this case was of a Hastelloy®-X material, nominally 1.6 mm in diameter. The actual joining configuration was similar to that described in Fig. 1. Welding was done with the same ASAP power supply and torch as shown in Fig. 2. A major difference for these trials was the use of enhanced shielding techniques. Since oxidation during deposition was a major concern, all deposition trials were done in a hard glove box, shown in Fig. 4. In this glove box, the dewpoint could be maintained below –70°C and 1-ppm oxygen. The power supply, torch, and any necessary tooling were placed in the chamber prior to conducting the deposition trials. The ESD setup included a Cu fixture with two restraining straps. In addition, Hastelloy® backing plates and run-off tabs were used to maintain both quality and geometry of the joint. Welding practices similar to those shown in Table 1 were used. This practice resulted in a peak current on the order of about 180 A and a pulse width of roughly 60 µs. Sample current waveforms

for the T-111 to MarM 247 and Mo-47%Re to MarM 247 practices are provided in Figs. 5 and 6, respectively. The process can be described as first buttering the refractory metal and MarM 247 with the Hastelloy®-X, and then filling in the remainder of the joint. In all cases, the back of the sample was also ESD filled to ensure final geometry of the specimen. Assembly of each tensile specimen took roughly 8 h. Samples for metallographic inspection were mechanically polished and subjected to a two-state etching process. The Ni-based superalloy half of the joint was etched with a 40% HCl, 30% $HNO_3$, 10% glycerol, 20% acetic acid solution. This solution allowed clear resolution of the retained solidification structure in these materials. The refractory alloy half of the joint was etched in a 20% HF, 10% $HNO_3$, 15% $H_2SO_4$, balance $H_2O$ solution that was effective in decorating grain and structural boundaries in these materials. Tensile testing was done on replicate samples of each configuration. Testing was done at the NASA Glenn Research Center (Ref. 18). Samples had the run-off tabs removed and were ground nominally flat. Testing was done to provide yield strengths, tensile strengths, and elongations to failure.

## Results

Welding of the MA957 samples was conducted using the procedures defined above. The surface of the resulting joint is shown in Fig. 7. The individual splats are evident, as well as the consistency of the final joint geometry. A cross section of the weld is provided in Fig. 8. The cross section clearly indicates that the joint morphology itself consists of a number of overlaid splats. These splats are of a very fine scale, not appreciably coarser than the grain size of the base material. The morphology of the joint also shows some dark bands, nominally running along the contour of the fill. These may be related to soot that becomes integrated into the joint with subsequent passes. It is also apparent that there is virtually no HAZ associated with this weld. Here, the base metal microstructure extends to within a few hundred microns of the first deposited splat layer.

Hardness variations across the joint are presented in Fig. 9. The base material shows a hardness level of nominally 330 VHN. Within the weld, hardness swings are noted. Peak hardnesses in excess of 350 VHN are observed within this weld, as well as values as low as 290 VHN. The high hardnesses in the weld are believed related to the fine splat morphology implicit in the fusion zone. The low hardness observations may be related to high levels of porosity within these welds as has been suggested elsewhere (Ref. 16). A single tensile test was done on one of these ESD joints due to limited material availability. The joint exhibited an ultimate strength of roughly 700 MPa, and failed along the FZ-HAZ interface. The strength here is about 65% that of the base material (Ref. 19). The resulting failed sample is shown in Fig. 10. The failure corresponds to the region of low hardness (in Fig. 9), and is probably the result of porosity as discussed previously. Finally, small angle neutron scattering (SANS) analysis was done elsewhere (Ref. 16) and suggests some redistribution of the nano-features. That work indicated the nano-features roughly doubled in size (2.4 to 4.7 nm) and decreased in density (0.6 to 0.12%) as a result of ESD processing. It was also suggested that this coarsening may have been partially responsible for the loss in properties seen in this part of the weld.


*Fig. 10 — ESD-welded MA957 sample after mechanical testing.*

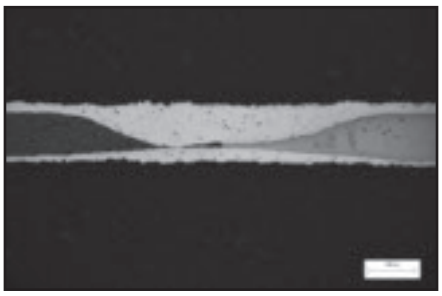

*Fig. 12 — Macrograph showing the overall morphology of an ESD-welded T-111 to MarM 247 specimen with a Hastelloy®–X filler.*

An example of a rewelded tensile refractory metal to Ni-based superalloy specimen is provided in Fig. 11. The morphology is quite similar to that seen for the MA 957 welding trials described previously. Joints are again relatively smooth and conform nominally to the overall shape of the part. This is characteristic of the fine splats deposited during ESD processing.

Macrographs of the T-111 to MarM 247 and Mo-47%Re to MarM 247 joints are provided in Figs. 12 and 13, respectively. The cross sections indicate minimal dilution, and relatively high density of the deposits. Deposition on both the scalloped and back sides of the joint can also be seen. These results suggested that interactions between the fill and the substrate were highly localized. This is can be observed in the higher magnification micrographs for representative T-111, Mo-47%Re, and MarM interfaces in Figs. 14–16, respectively. Results for deposition of the Hastelloy®-X onto the two refractory metals indicate little change to the substrates, with splats nominally 5 μm thick apparently wetting the surfaces. In this case, any compositional changes must be considered over this first layer of splats. For the deposit onto the Mar-M 247 alloy (Fig. 16), there is clearly some mixing and compositional transition. However, this transition again appears to be limited to the first one or two layers of splats (10–15 μm).


*Fig. 11 — An as ESD-welded refractory metal to Ni-based superalloy tensile specimen.*

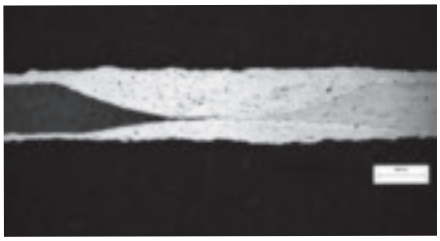

*Fig. 13 — Macrograph showing the overall morphology of an ESD-welded Mo-47%Re to MarM 247 specimen with a Hastelloy®–X filler.*

Duplicate tensile tests were made for each of these joint combinations. Yield, tensile, and elongation results are provided for each joint tested in Table 2. The T-111 to MarM 247 joints showed yield strengths above 600 MPa, tensile strengths near 700 MPa, and elongations ranging from roughly 5 to 9%. Alternately, the Mo-47%Re to MarM 247 joints showed both yield and tensile strengths of roughly 800 MPa, with little elongation (~0.5%). The results here are compared with mechanical properties data for each material (T-111, Mo-47%Re, MarM 247, Hastelloy X) from standard literature sources (Refs. 20–23). These results are presented in

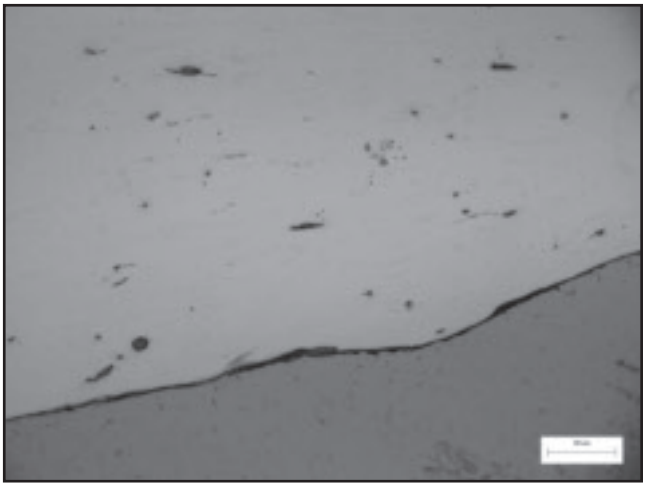

*Fig. 14 — Details of the T-111 substrate to Hastelloy®–X fusion zone interface following ESD welding.*

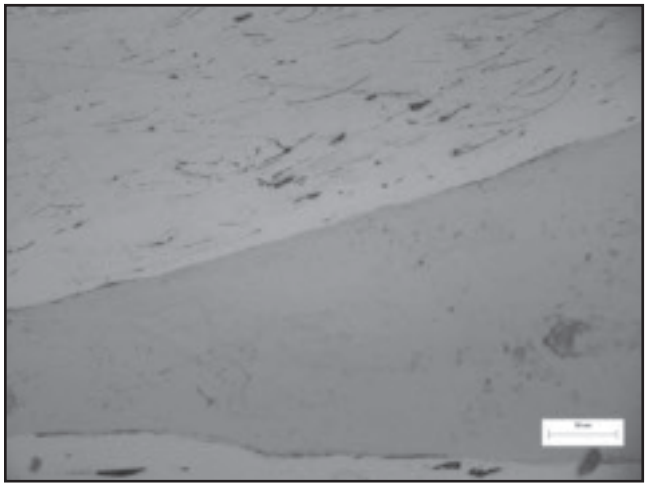

*Fig. 15 — Details of the Mo-47%Re substrate to Hastelloy®–X fusion zone interface following ESD welding.*

Table 3. In each case, the yield strength of the weld corresponds to the weaker of the two attached substrates, rather than the Hastelloy®–X filler.

## Discussion

### Cooling Rates during Electro-Spark Deposition

As suggested previously, a key characteristic of electro-spark deposition is the high implicit cooling rates associated with the technology. Some estimation of these cooling rates can be achieved from simple thermal analysis. During ESD, it is understood that liquid droplets of the filler metal are formed by individual percussive actions (Ref. 8), resulting in the observed individual splats. The thermal analysis involves interpreting the behavior of the individual molten splat as it impinges on the surface. This is essentially a one-dimensional heat transfer problem, in which the heat of fusion is conducted away from the splat into the metal substrate. The governing equation here is of the form

$$\frac{T(x,t)-T_o}{T_i-T_o} = erf\left(\frac{x}{2\sqrt{\alpha t}}\right) \quad (1)$$

Where $T(x,t)$ is the temperature as a function of displacement into the substrate $(x)$, and time after splat impact $(t)$, $T_i$ and $T_o$ are the initial (melting) temperature of the splat and the ambient temperature, and $\alpha$ is the thermal diffusivity. The boundary condition for this construct can then be established by matching the thermal gradient into the substrate to the available heat of fusion in the splat. This can be expressed as

$$-kA\left.\frac{dT}{dx}\right|_{x=0} = \frac{d}{dt}\left(fH_m\rho x_{sp}A\right) \quad (2)$$

Where $k$ is the material thermal conductivity, $\rho$ is the density, $x_{sp}$ is the splat thickness, $H_m$ is the heat of fusion, and $f$ is the fraction molten material remaining in the splat. The former expression can also be differentiated to define the thermal gradient in the substrate. This has the following form:

$$\left.\frac{dT}{dx}\right|_{x=0} = \left.\frac{\partial T}{\partial x}\right|_{x=0} = \left.\frac{T_i-T_o}{\sqrt{\pi\alpha t}}e^{\frac{-x^2}{4\alpha t}}\right|_{x=0} = \frac{T_i-T_o}{\sqrt{\pi\alpha t}} \quad (3)$$

For $t > 0$. The latter form of Equation 3 then can be combined with Equation 2, and reorganized to provide the following integral relationship:

$$\int_0^{t_f}\frac{T_i-T_o}{\sqrt{\pi\alpha t}}dt = -\frac{x_{sp}H_m}{\alpha C_p}\int_1^0 df \quad (4)$$

In this equation, $t_f$ is the time for an individual splat to solidify. $C_p$ (heat capacity) has also been substituted into this equation for $k$ and $\rho$ using the relationship $\alpha=k/\rho C_p$. This equation can then be integrated to define the time required for an individual splat to solidify. This has the form

$$t_f = \frac{\pi}{4\alpha}\left(\frac{x_{sp}H_m}{C_p\left(T_i-T_o\right)}\right)^2 \quad (5)$$

$t_f$ then defines the transition between heat flow defined by the heat of fusion, and that is defined by changes in the heat capacity of the splat and surrounding system. Prior to $t_f$, the splat itself was of the nominal melting temperature ($T_m$). Following $t_f$, changes in the temperature distribution are heat capacity driven. The boundary condition at the interface between the splat and substrate then becomes

**Table 2 — Mechanical Properties of Sample ESD-Welded Refractory Metal to MarM 247 Joints**

| Refractory Metal | Ni-Based Superalloy | YS (MPa) | UTS (MPa) | Elongation (%) |
|---|---|---|---|---|
| Mo-47%Re | MarM 247 | 813 | 817 | 0.6 |
| Mo-47%Re | MarM 247 | 784 | 807 | 0.4 |
| T-111 | MarM 247 | 611 | 682 | 4.7 |
| T-111 | MarM 247 | 607 | 683 | 8.5 |

**Table 3 — Representative Mechanical Properties of Each Material Substrate and Filler Used in the ESD Refractory Metal to MarM 247 Welding Trials**

| Material | YS (MPa) | UTS (MPa) | Reference |
|---|---|---|---|
| MarM 247 | 828 | 966 | (19) |
| Mo-47%Re | 848 | 1034 | (20) |
| T-111 | 613 | 679 | (21) |
| Hastelloy® X | 379 | 767 | (22) |

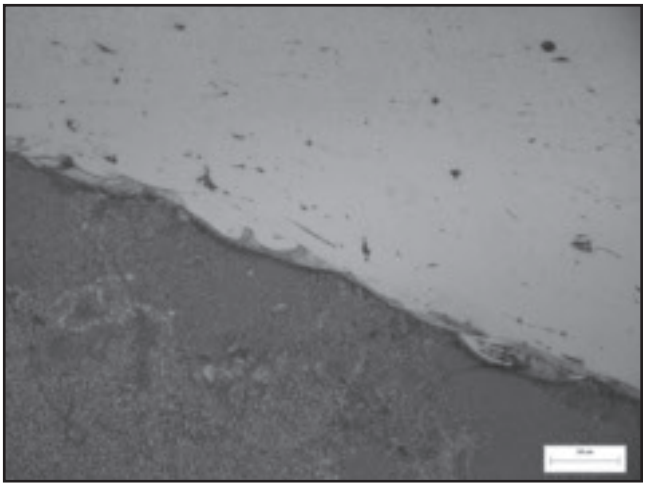

*Fig. 16 — Details of the MarM 247 substrate to Hastelloy®–X fusion zone interface following ESD welding.*

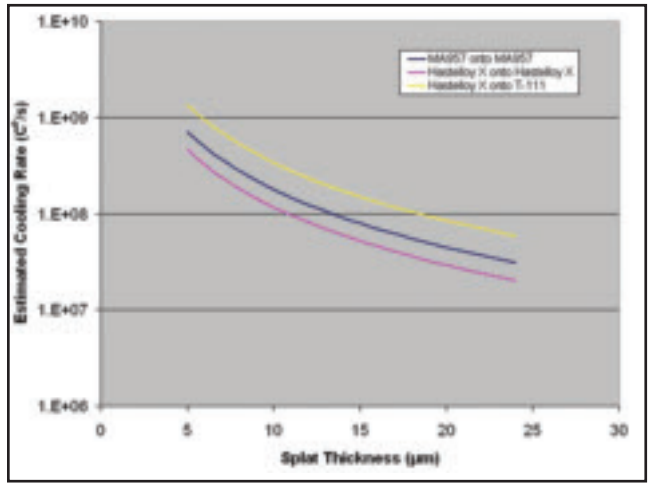


*Fig. 17 — Cooling rates as a function of ESD splat thickness for the three applications under study. Cooling rates are calculated from the thermal analysis done as part of this work.*

$$-kA\frac{dT}{dx}\bigg|_{x=0} = \rho C_p x_{sp} A\frac{dT}{dt} \qquad (6)$$

Combining Equations 3, 5, and 6 then yields the following cooling rate expression:

$$\frac{dT}{dt} = \frac{2\alpha C_p}{\pi x_{sp}^2 H_m}\left(T_m - T_o\right)^2 \qquad (7)$$

This corresponds to peak cooling rates occurring at the termination of solidification of the splat. For comparison purposes, Equation 7 has been used to plot implicit cooling rate results for a number of the applications described in this paper. Material thermal properties for these applications are estimated from data available in the literature (Refs. 23–25), and are provided in Table 4. These results are shown in Fig. 17. Most notable, cooling rates here are seen to range from roughly $10^{8}$°C/s to $10^{9}$°C/s. This is considerably higher than the $10^{5}$°C/s to $10^{6}$°C/s rates reported previously (Ref. 9). It must be remembered, however, that these cooling rates represent those occurring at the instant of solidification, and will moderate rapidly at lower temperatures. The results shown in Fig. 17 do indicate the influence of splat thickness, as well as the substrate and deposited materials used. These results suggest first that a doubling in the resulting splat thickness can reduce cooling rates by an order of magnitude. Also, it appears depositing MA957 or Hastelloy X onto similar material substrates results in similar cooling rates. This is not surprising, in that thermal properties are similar for these two material systems (Table 4). However, cooling rates increase by roughly a factor of three when the Hastelloy® X is deposited onto the tantalum substrate. This appears related to the high thermal diffusivity associated with the substrate material.

### Metallurgical Implications of ESD Welding

Electro-spark deposition, as indicated previously, accomplishes material transfer through melting and resolidification of discrete volumes of material. These volumes are necessarily small, resulting in the 1- to 5-µm splat thicknesses shown in the two applications presented. The analysis shown here suggests that implicit cooling rates for these splats can be as high as $10^{8}$°C/s to $10^{9}$°C/s at the terminus of solidification. Observations of other researchers have suggested that solidification of the splats occurs with a fine dendritic structure (Ref. 26). This observation is consistent with the experience of this author. The morphology of the splats, consistent with the results presented in this work, also appears to occur without identifiable segregation. To understand this solidification behavior, it is helpful to look to related process technologies, particularly MPW. As suggested previously, MPW shows similar thermal cycles and solidification morphologies (melt zone thicknesses) as seen on the individual splats during ESD. Recent work (Ref. 27) has been done evaluating chemical compositions of resolidified melt zones during MPW Al to Cu and Al to steel. That work has shown that the composition of the melt zone is uniform, apparently devoid of local segregation. While the authors of that work suggest that the resulting compositions may be intermetallic related, they do not match up to any intermetallic in the systems studied. This work can also be seen as verification of rapid solidification without segregation.

The implication of such observations is that the solidification times during ESD (or other impulse processes) are sufficiently short that the concept of local equilibrium has broken down. Local equilibrium is the mechanism (Ref. 28) of segregation during solidification, and is one of the contributors to the instabilities that lead to cell/dendrite formation (Ref. 29). Without sufficient time for this segregation to occur, the material behaves as a pure material, with the scale of the solidification structure driven by surface tension (Ref. 28). Impulse processes then offer the potential for solidification without compositionally driven cracking mechanisms (Ref. 30). Further, such extreme cooling rates also offer potential for

**Table 4 — Thermal Properties for Each of the Materials under Evaluation during the Modeling Studies (410 SS properties are used in lieu of available values for MA957)**

| Thermal Property | 410 SS[(a)] | Material Hastelloy X | T-111 |
|---|---|---|---|
| $\alpha$(m²/s) = | $7.57\times10^{-6}$ | $7.74\times10^{-6}$ | $2.24\times10^{-5}$ |
| $C_p$(J/kg-°C) = | 460 | 440 | 150 |
| $H_m$(J/kg) = | $2.72\times10^{5}$ | $3.06\times10^{5}$ | $1.70\times10^{5}$ |
| k(W/m-C) = | 26.9 | 27.2 | 56 |
| p(kg/m³) = | 7730 | 7990 | 16650 |
| $T_m$(°C) = | 1505 | 1310 | 2996 |

(a) 410 SS is used as a substitute here for MA957.

suppressing diffusion-based solid-state phase transformations. This offers additional potential for avoiding deleterious phase formation. It is not surprising then, that impulse technologies are often applied to dissimilar combinations. Successful MPW Al to Cu (Refs. 13, 27), Al to steel (Ref. 27), percussion welding Ag to Cu, and even ESD of complex coatings (Refs. 3, 6, 13) all demonstrate the capabilities of these technologies. Indeed, ESD welding has been found useful for the applications described due to the homogeneity of the deposit, and minimization of any transition zones between materials.

Electro-spark deposition, of course, achieves these high cooling rates by depositing microvolumes of metal onto a nominally cold substrate. Clearly, the benefits of the technology are reduced as the deposition rate increases. In fact, ESD only appears to be functional at deposition rates in the milligram/minute range. As a result, using this process to create joints is a time-intensive process (multiple hours to create a single thin-gauge tensile coupon). Further, these joints must consist of hundreds, if not thousands of overlaid deposits (splats).

The required processing suggests that ESD welding is limited in its applications. These inevitably will be very high value-added applications, where material compatibility is a major joining challenge. A transition joint between refractory metals and cast Ni-based superalloys is one such example. Similarly, complex material systems that react adversely to welding thermal cycles are another potential application such as the MA957 application described previously. Finally, the process may be adaptable where automation (providing the multiple overlays required to achieve a joint) can be used. An example of this is transition joints, which can be made to a relatively simple geometry and then adapted into a larger configuration.

## Conclusions

Electro-spark deposition welding is an adaptation of ESD for the attachment of complex material substrates. Thermal cycles during ESD are analogous to other impulse-type processes, including percussion welding and MPW. As a result, deposits made during ESD processing have extremely high implicit cooling rates. Analysis conducted here suggests these cooling rates can be on the order of $10^{8\circ}$ to $10^{9\circ}$C/s at the terminus of splat solidification. These high implicit cooling rates are seen as enablers to joining metallurgically complex materials, as well as substrate combinations that are metallurgically incompatible. Work here has demonstrated two such applications. The first is the attachment of new grades of mechanically alloyed (MA957) stainless steels. The second is dissimilar material attachments between refractory metals and cast Ni-based superalloys. Successful joints were made in both cases. MA957 joints were made with some coarsening of the nano-features, but overall exhibited a refined microstructure. Refractory metal joints were made with strengths approaching that of the weaker of the two base materials joined. The approach is technically feasible for a wide range of materials and combinations currently not able to be joined today. However, the process is exceptionally slow (single digit milligram/minute deposition rates), and must be limited to extremely high-value applications, where materials joining is exceedingly problematic. Potential applications include transition joints for dissimilar material combinations, and those of sufficient simplicity that extensive automation can be employed.

*Acknowledgments*

The author would like to thank Frank Ritzert of the NASA Glenn Research Center and Robert Miller of DDL Omni for their support of this work.

*References*

1. Rawdon, H. S. 1924. *Transactions of the American Institute of Mechanical Engineering*, 79:37.

2. Sheldon, G. L., and Johnson, R. N. 1985. Electro-spark deposition — A technique for producing wear resistant coatings. *Wear of Materials 1985*, ASME, New York, N.Y.

3. Johnson, R. N., and Sheldon, G. L. 1986. Advances in the electrospark deposition coating process. *Journal of Vacuum Science & Technology A* 4(6): 2740–2746.

4. Johnson, R. N. 1988. Principles and applications of electro-spark deposition. *Surface Modification Technologies*, TMS, Warrendale, Pa.

5. Galinov, I. V., and Luban, R. B. 1996. Mass transfer trends during electrospark alloying. *Surface Coatings and Technology* 79: 9–18.

6. Wand, P.-Z., Pan, G.-S., Zhou, Y., Qu, J.-X., and Shao, H.-S. 1997. Accelerated electrospark deposition and the wear behavior of coatings. *Journal of Materials Engineering and Performance* 6(6): 780–784.

7. Li, Z., Gao, W., Kwok, P., Li, S., and He, Y. 2000. *High Temperature Materials and Processes* 19(6): pp. 443–458.

8. Reynolds, J. L., Holdren, R. L., and Brown, L. E. 2003. Electro-spark deposition. *Advanced Materials and Processes*, 161(3), ASM International, Materials Park, Ohio.

9. Cadney, S., and Brochu, M. 2008. Formation of amorphous Zr41.2Ti13. 8Ni10Cu12.5Be22.5 coatings via the electrospark deposition process. *Intermetallics* 16(4): 518–523.

10. Gould, J. E., Khurana, S. P., and Li, T. 2006. Predictions of microstructures when welding automotive advanced high-strength steels. *Welding Journal* 85(5): 111-s to 116-s.

11. Wilson, R. D. 1995. Rapid solidification joining of silver electrical contacts to copper conductors using the capacitor discharge welding process. *Advances in Welding Processes, Proceedings of the Eleventh Annual North American Research Conference*, Edison Welding Institute, Columbus, Ohio.

12. Gould, J. E., Zhang, P., and Kimchi, M. 2003. Development of magnetic pulse welding technology for automotive applications. EWI Research Report 44587CPQ/R-2/03, Edison Welding Institute, Columbus, Ohio.

13. Seregeeva, Y. U. A., Chudakov, V. A., and Gordon, G. N. 1989. Examination of the transition zone in magnetic pulse welded joints between aluminium and copper. *Paton Weld. J.* 1(12): 874–877.

14. Stern, A., and Aizenshtein, M. 2002. Bonding zone formation in magnetic pulse welds. *Science and Technology of Welding and Joining* 7(5): 339–342.

15. Gould, J. E., Castner, H. R., Kimchi, M., Kristan, J. V., Maitland, S. B., Reynolds, J., and Zhang, P. 2007. Chapter 15 – Other welding and cutting processes. *Welding Handbook*, Ninth Edition, Vol. 3, Part 2, pp. 561–615, American Welding Society, Miami, Fla.

16. Miao, P., Odette, G. R., Gould, J., Bernath, J., Miller, R., Alinger, M., and Zanis, C. 2007. The microstructure and strength properties of MA957 nanostructured ferritic alloy joints produced by friction stir and electrospark deposition welding. *Journal of Nuclear Materials* 367-370: 1197–1202.

17. Gould, J. E., Ritzert, F. J., and Loewenthal, W. S. 2006. Preliminary investigations of joining technologies for attaching refractory metals to Ni-based superalloys. *Space Technology and Applications International Forum 2006* Springer-Verlag, N.Y., Secaucus, N.J.

18. Ritzert, F. 2006. Private communication.

19. Alinger, M. J., Odette, G. R., and Hoelzer, D. T. 2004. *Journal of Nuclear Materials* 382: 329–333.

20. DiStefano, J. R., and McCoy, H. E. 2002. Mechanical properties of T-111 at low to intermediate temperatures. *International Journal of Refractory Metals & Hard Materials* Vol. 20, pp. 381–387.

21. Carlen, J.-C., and Bryskin, B. D. 1994. Rhenium — A unique rare metal. *Materials and Manufacturing Processes* 9(6): 1087–1104.

22. Sink, L. W., Hoppin III, G. S., and Fujii, M. 1979. Low-cost directionally solidified turbine blades. NASA CR-159464, AiResearch 21-2953, pp. 243–247.

23. *Hastelloy® X Alloy.* 1997. Haynes International, Inc., Kokomo, Ind.

24. Goldberg, D. C. 1969. *Aerospace Structural Metals Handbook*, AFML-TR 68–115.

25. 1996–2011. *www.matweb.com*. MatWeb LLC, Blacksburg, Va.

26. Gao, W., and Li, Z. 2008. Nano-structured alloy and composite coatings for high temperature applications. *Materials Research* 7(1): 175–182.

27. Zhang, Y., Babu, S. S., Prothe, C., Blakely, M., Kwasegroch, J., LaHa, M., and Daehn, G. S. 2010. Application of high velocity impact welding at varied different length scales. *J. Mater. Process. Tech*.

28. Flemings, M. C. 1974. *Solidification Processing*, McGraw Hill, New York, N.Y.

29. Mullins, W. W., and Skerka, R. F. 1964. Stability of a planar interface during solidification of a dilute binary alloy. *Journal of Applied Physics*. 35(2): 444–451.

30. Kou, S. 1987. *Welding Metallurgy*, Wiley-Interscience, New York, N.Y.